

# The 6dFGS peculiar velocity field

Christopher M. Springob,<sup>1,2,3</sup> Christina Magoulas,<sup>4</sup> Matthew Colless,<sup>3</sup>  
D. Heath Jones,<sup>5</sup> Lachlan Campbell,<sup>6</sup> John Lucey,<sup>7</sup> Jeremy Mould,<sup>8</sup>  
and Pirin Erdoğdu<sup>9</sup>

<sup>1</sup>International Centre for Radio Astronomy Research, The University of Western Australia,  
Australia

email: christopher.springob@icrar.org

<sup>2</sup>ARC Centre of Excellence for All-Sky Astrophysics; <sup>3</sup>Australian Astronomical Observatory;

<sup>4</sup>University of Melbourne, Australia; <sup>5</sup>Monash University, Australia;

<sup>6</sup>University of Western Kentucky, USA; <sup>7</sup>University of Durham, UK;

<sup>8</sup>Swinburne University, Australia; <sup>9</sup>University College London, UK

**Abstract.** The 6dF Galaxy Survey (6dFGS) is an all-southern-sky galaxy survey, including 125,000 redshifts and a Fundamental Plane (FP) subsample of 10,000 peculiar velocities. This makes 6dFGS the largest peculiar-velocity sample to date. We have fitted the FP with a trivariate Gaussian model using a maximum-likelihood approach, and derive the Bayesian probability distribution of the peculiar velocity for each of the 10,000 galaxies. We fit models of the velocity field, including comparisons to the field predicted from the redshift-survey density field, to derive the values of the redshift-space distortion parameter  $\beta$ , the bulk flow and the residual bulk flow in excess of that predicted from the density field. We compare these results to those derived by other authors and discuss the cosmological implications.

**Keywords.** surveys, galaxies: distances and redshifts, cosmological parameters, large-scale structure of universe

---

## 1. Introduction

6dFGS is a combined redshift and peculiar-velocity survey of galaxies covering the entire southern sky at  $|b| > 10^\circ$  (Jones *et al.* 2009). While the redshift survey includes more than 125,000 galaxies, the peculiar-velocity subsample (hereafter 6dFGSv) includes  $\sim 10,000$  of those galaxies, extending in redshift to  $cz \sim 16,500 \text{ km s}^{-1}$ . This represents the largest peculiar-velocity sample from a single survey to date.

The peculiar velocities are derived from Fundamental Plane (FP) data for those galaxies, with spectroscopy from the UK Schmidt Telescope and photometry from the Two Micron All-Sky Survey (2MASS) Extended Source Catalog (Jarrett *et al.* 2000). When plotted in the 3D parameter space with axes  $r = \log(R_e)$ ,  $s = \log(\sigma)$  and  $i = \log(I_e)$ —where  $R_e$ ,  $\sigma$  and  $I_e$  represent effective radius, central velocity dispersion and effective surface brightness, respectively—the galaxies lie along a plane which can be expressed in the form  $r = as + bi + c$ , where  $a$ ,  $b$  and  $c$  are observationally derived constants. Because  $r$  is a distance-dependent quantity, and both  $s$  and  $i$  are nearly distance-independent, the FP can be used as a distance indicator, with the galaxy's offset from the FP along the  $r$  direction representing a measure of the galaxy's peculiar velocity.

## 2. Data

The details of the sample selection and data reduction are presented in L. Campbell *et al.* (in prep.) and Magoulas *et al.* (2012). In brief, the 6dFGSv includes the  $\sim 10,000$

6dFGS early-type galaxies with spectral signal-to-noise ratios greater than five, heliocentric redshift  $z_{\text{helio}} < 0.055$ , velocity dispersion greater than  $112 \text{ km s}^{-1}$ , and  $J$ -band magnitude brighter than  $m_J = 13.65$  mag. Here, ‘early-type galaxies’ include both elliptical galaxies and spiral bulges in cases where the bulge fills the 6dF fibre. The galaxies were identified as ‘early-type’ by matching the observed spectrum, through cross-correlation, to template galaxy spectra. Each galaxy image was subsequently examined by eye, and galaxies were removed from the sample if the morphology was irregular, the galaxy appeared to be a spiral with an obvious dust lane or the fibre aperture was contaminated by a star, another galaxy or a galaxy disk.

We also removed from the sample several hundred galaxies within the heliocentric redshift limit of  $z_{\text{helio}} = 0.055$  that nonetheless have recessional velocities greater than  $16,120 \text{ km s}^{-1}$  in the cosmic microwave background (CMB) reference frame. This was done because our peculiar-velocity analysis is carried out in the CMB frame, and we wish the survey to cover a symmetric volume within the southern hemisphere in that frame. Since the initial survey redshift limit is made in the heliocentric reference frame, we must limit the sample to  $16,120 \text{ km s}^{-1}$  to maintain the same redshift limit across the entire southern hemisphere.

Velocity dispersions were measured from the 6dFGS spectra. The apparent magnitudes were taken from the 2MASS Extended Source Catalog. We derived the angular radii and surface brightnesses from the 2MASS images in the  $J$ ,  $H$  and  $K$  bands for each of the galaxies in the sample, taking the total magnitudes from the 2MASS catalog, and then measuring the location of the isophote that corresponds to the half-light radius. Surface brightness as defined here is then taken to be the average surface brightness interior to the half-light radius. We use the  $J$ -band values, since they offer the smallest photometric errors.

To help interpret our velocity-field results, we would like to compare them to a predicted velocity field, constructed using the redshift-space distribution of galaxies and assuming that the matter distribution traces the galaxy distribution.

One of the largest, most complete reconstructed velocity fields at present is derived from galaxies in the Two-Micron All-Sky Redshift Survey (2MRS). In the final data release (Huchra *et al.* 2012), the 2MRS contains measured redshifts for 44,699 galaxies with a magnitude limit of  $K_s = 11.75$  mag. The dense, all-sky sampling of 2MRS provides an ideal counterpart for comparison of the predicted velocity field with the dense, homogeneous sampling of the observed 6dFGS galaxies, given the significant overlap in the southern hemisphere. Hence, we choose the 2MRS reconstructed density and velocity fields of Erdoğdu *et al.* (2012; updated from Erdoğdu *et al.* 2006), which uses the 2MRS redshift sample to recover the linear-theory predictions for density and velocity. The method of reconstruction is outlined in Erdoğdu *et al.* (2006; it closely follows the method of Fisher *et al.* 1995), where it was applied to a smaller 2MRS sample of 20,860 galaxies with a brighter magnitude limit of  $K_s = 11.25$  mag and a median redshift of  $6000 \text{ km s}^{-1}$ . It relies on the assumption that the matter distribution traces the galaxy distribution in 2MRS, with a bias parameter such that  $\beta = \Omega_m^{0.55}/b = 0.4$ . The reconstruction gives us velocity vectors which are plotted on a grid in Supergalactic Cartesian coordinates, with grid points spaced apart by  $8 \text{ Mpc } h^{-1}$ , extending out to a distance of  $196 \text{ Mpc } h^{-1}$  in each direction.

### 3. Fitting the Fundamental Plane

To fit the FP, we follow a maximum-likelihood method analogous to the method used to fit the FP for EFAR (Colless *et al.* 2001). The method is explained in detail in Magoulas *et al.* (2012), but we briefly summarize the approach here.

As Colless *et al.* (2001) note, when plotted in  $r-s-i$  space, the galaxies follow a 3D Gaussian distribution. Therefore, our maximum-likelihood method involves fitting the distribution of galaxies in  $r-s-i$  space to a 3D Gaussian of which the two longest axes define the FP and the shortest axis is orthogonal to the plane.

Given this functional form, the probability density for the  $i^{\text{th}}$  galaxy,  $P(\mathbf{x}_i)$ , can be computed according to Magoulas *et al.* (2012, their eq. 4) as

$$P(\mathbf{x}_n) = \frac{\exp[-\frac{1}{2}\mathbf{x}_n^T(\boldsymbol{\Sigma} + \mathbf{E}_n)^{-1}\mathbf{x}_n]}{(2\pi)^{\frac{3}{2}}|\boldsymbol{\Sigma} + \mathbf{E}_n|^{\frac{1}{2}}f_n}, \quad (3.1)$$

where  $\boldsymbol{\Sigma}$  is the FP variance matrix,  $\mathbf{E}_n$  the observational error matrix and  $\mathbf{x}_n$  the position  $(r - \bar{r}, s - \bar{s}, i - \bar{i})$  in FP space. In logarithmic form, this is written as

$$\ln[P(\mathbf{x}_n)] = -\left[\frac{3}{2}\ln(2\pi) + \ln(f_n) + \frac{1}{2}\ln(|\boldsymbol{\Sigma} + \mathbf{E}_n|) + \frac{1}{2}\mathbf{x}_n^T(\boldsymbol{\Sigma} + \mathbf{E}_n)^{-1}\mathbf{x}_n\right]. \quad (3.2)$$

The 3D Gaussian is defined by eight parameters, i.e. the slopes  $a$  and  $b$ , the mean values of the FP parameters  $\bar{r}, \bar{s}, \bar{i}$  and the intrinsic scatter along the 3D Gaussian axes,  $\sigma_1, \sigma_2, \sigma_3$ . As previously mentioned,  $\mathbf{x}_n$  is a function of both the observable parameters  $r, s$  and  $i$ , and the FP model parameters  $\bar{r}, \bar{s}$  and  $\bar{i}$ . Likewise,  $\mathbf{E}_n$  and  $\boldsymbol{\Sigma}$  depend on  $a, b, \sigma_1, \sigma_2$  and  $\sigma_3$ . Our maximum-likelihood fitting method involves searching the values of the eight fitted parameters that maximize the total likelihood,

$$\ln(L) = \sum_n \ln[P(\mathbf{x}_n)]. \quad (3.3)$$

This is done by searching the multi-dimensional parameter space with a non-derivative multi-dimensional optimization algorithm called BOBYQA (Bound Optimization BY Quadratic Approximation; Powell 2006).

The best-fitting coefficients to the  $J$ -band FP,  $r = as + bi + c$ , are  $a = 1.524 \pm 0.026$ ,  $b = -0.885 \pm 0.008$  and  $c = -0.329 \pm 0.054$ , where  $r, s$  and  $i$  are given in units of  $\log[\text{kpc } h^{-1}]$ ,  $\log[\text{km s}^{-1}]$  and  $\log[\text{L}_\odot/\text{pc}^2]$ , respectively. (Note, the ‘ $h$ ’ in  $\text{kpc } h^{-1}$  refers to the Hubble constant in units of  $100 \text{ km s}^{-1} \text{ Mpc}^{-1}$ . For the purpose of angular-unit conversion, a flat cosmology of  $\Omega_m = 0.3$  and  $\Omega_\Lambda = 0.7$  is assumed, although the specifics of the assumed cosmology affect the FP fit only very weakly.)

### 4. Derivation of the peculiar velocities

Rather than calculating individual peculiar velocities with error bars, we calculate Bayesian posterior probability distributions for each galaxy. This Bayesian approach is then implemented in the following manner:

(1) Specify the FP template relation. We know that the FP is a plane of the form  $r = as + bi + c$ , but for the purpose of measuring the distances and peculiar velocities, we need to know the full distribution of objects in FP space. Therefore, for our 3D Gaussian model, we need to specify the values of all eight parameters  $(a, b, \bar{r}, \bar{s}, \bar{i}, \sigma_1, \sigma_2, \sigma_3)$ . These are provided in Magoulas *et al.* (2012). For the  $J$ -band sample,  $a = 1.523$ ,  $b = -0.885$ ,  $\bar{r} = 0.184$ ,  $\bar{s} = 2.188$ ,  $\bar{i} = 3.188$ ,  $\sigma_1 = 0.053$ ,  $\sigma_2 = 0.318$  and  $\sigma_3 = 0.170$ .

(2) For each individual galaxy  $n$ , loop through every possible logarithmic comoving distance  $d_{H,n,i}$  that the galaxy could have. Distance is, of course, a continuous quantity.

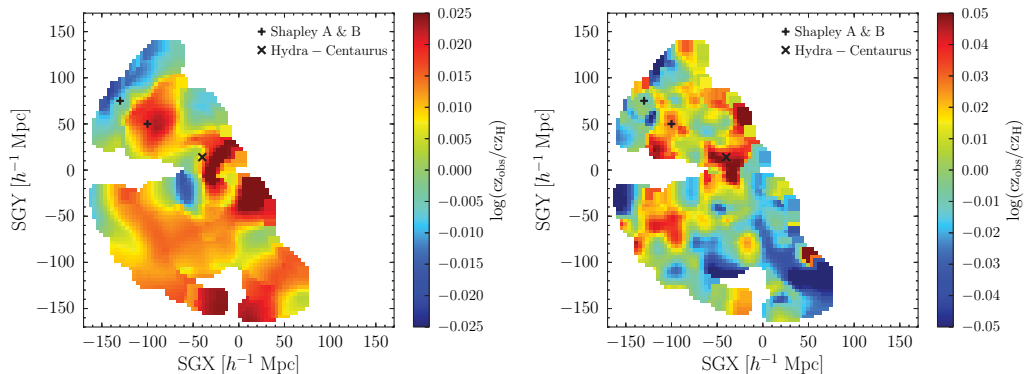


**Figure 1.** Smoothed peculiar-velocity field in a slice through the Supergalactic plane ( $-20 < \text{SGZ} < +20 \text{ Mpc } h^{-1}$ ). On the left we show the predicted field from the 2MRS reconstruction. On the right we show the observed field from 6dFGS. The smoothing is on a grid with  $4 \text{ Mpc } h^{-1}$  grid spacing, but only the grid points with nearby galaxies are shown. The points are colour-coded by the logarithm of the ratio of redshift distance to real distance, which represents peculiar velocity in logarithmic units. Redder (bluer) colours correspond to more positive (negative) peculiar velocities. We also mark the positions of the Hydra–Centaurus Supercluster and of the two main concentrations of the Shapley Supercluster.

However, in practice, we are limited to examining a finite number of possible distances. Therefore, for the  $n^{\text{th}}$  galaxy, we consider a finite set of possible values of logarithmic comoving distance, with index  $i$ .

(3) We calculate the probability density for each of those possible logarithmic comoving distances by calculating the probability density for the corresponding physical radius, as given by Eq. (3.2). This probability density as a function of radius directly translates into a probability density with distance.

## 5. Peculiar Velocity Field Cosmography

We used adaptive kernel smoothing to smooth the peculiar-velocity probability distributions onto a Cartesian grid in Supergalactic Cartesian coordinates, with  $4 \text{ Mpc } h^{-1}$  grid spacing. We do this both for the 6dFGS and for the reconstructed 2MRS velocity fields, as shown in Fig. 1. Our observed velocity field matches the predicted field in that we observe infall towards the Shapley Supercluster. However, we observe a stronger dipole motion in the general direction of Shapley as well, with disproportionately negative peculiar velocities in the bottom right-hand quadrant.

## 6. Peculiar Velocity Field Cosmology

In Magoulas (2012) we fit the observed field to the predicted field using a maximum-likelihood method. In doing so, we measure the value of the redshift-space distortion parameter,  $\beta = 0.29 \pm 0.06$ . This is smaller than, but still within the errors of, most other measured values for 2MRS. We have also fitted the value of the bulk flow for our sample, and find a value of  $337 \pm 66 \text{ km s}^{-1}$  towards  $(l, b) = (313^\circ \pm 9^\circ, 15^\circ \pm 10^\circ)$ , which is somewhat closer to the direction of the Shapley Supercluster than most other estimates of the bulk flow. We also fit a final model in which the observed velocity field is given by the 2MRS prediction plus a residual bulk flow. We find that the residual bulk flow is  $272 \pm 45 \text{ km s}^{-1}$  towards  $(l, b) = (326^\circ \pm 9^\circ, 37^\circ \pm 14^\circ)$ , which is also close to the direction of Shapley. The large residual bulk flow suggests that a large fraction of

the bulk flow is either induced by structures outside the survey volume or by structures within the survey volume that are being underestimated.

## References

- Colless, M., Saglia, R. P., Burstein, D., Davies, R. L., McMahan, R. K., & Wegner, G. 2001, *MNRAS*, 321, 277
- Erdođdu, P., Lahav, O., Huchra, J. P., et al. 2006, *MNRAS*, 373, 45
- Fisher, K. B., Lahav, O., Hoffman, Y., Lynden-Bell, D., & Zaroubi, S. 1995, *MNRAS*, 272, 885
- Huchra, J. P., Macri, L. M., Masters, K. L., et al. 2012, *ApJS*, 199, 26
- Jarrett, T. H., Chester, T., Cutri, R., Schneider, S., Skrutskie, M., & Huchra, J. P. 2000, *AJ*, 119, 2498
- Jones, D. H., Read, M. A., Saunders, W., et al. 2009, *MNRAS*, 399, 683
- Magoulas, C. 2012, Ph.D. Thesis, University of Melbourne, Australia
- Magoulas, C., Springob, C. M., Colless, M., et al. 2012, *MNRAS*, 427, 245
- Powell, M. J. D. 2006, in: *Large-Scale Nonlinear Optimization* (Roma, M., & Di Pillo, G., eds), Springer: New York, pp. 255–297